Article

Structure

Structural Plasticity of Methyllysine Recognition by the Tandem Tudor Domain of 53BP1

Graphical Abstract

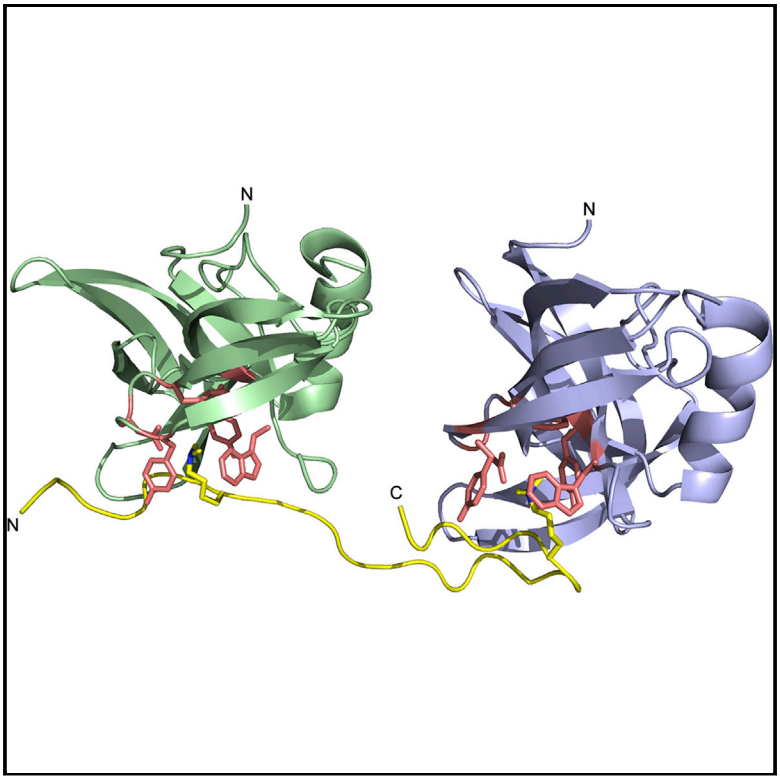

Authors

Qiong Tong, Gaofeng Cui, ..., Georges Mer, Tatiana G. Kutateladze

Correspondence

mer.georges@mayo.edu (G.M.), tatiana.kutateladze@ucdenver.edu (T.G.K.)

In Brief

Posttranslational modifications (PTMs) on p53 mediate function, stability, and localization of this tumor suppressor. Using biochemical and structural analyses, Tong et al. demonstrate that the dimeric tandem Tudor domain of 53BP1, a p53 cofactor, can interact with two methyllysine PTMs on a single p53K370me2K382me2 peptide.

Highlights

- Tandem Tudor domain (TTD) of 53BP1 uses different mechanisms to bind methylated PTMs
- The TTD selects for p53K382me2, H4K20me2, and H3K36me2
- Linked 53BP1 TTD can recognize dual methyllysine PTM

Accession Numbers

2MWO
2MWP

Tong et al., 2015, Structure *23*, 312–321
February 3, 2015
http://dx.doi.org/10.1016/j.str.2014.11.013

CellPress

Structure
Article

Structural Plasticity of Methyllysine Recognition by the Tandem Tudor Domain of 53BP1

Qiong Tong,[1,5] Gaofeng Cui,[2,5] Maria Victoria Botuyan,[2] Scott B. Rothbart,[3] Ryo Hayashi,[4] Catherine A. Musselman,[1] Namit Singh,[2] Ettore Appella,[4] Brian D. Strahl,[3] Georges Mer,[2,*] and Tatiana G. Kutateladze[1,*]

[1]Department of Pharmacology, University of Colorado School of Medicine, Aurora, CO 80045, USA
[2]Department of Biochemistry and Molecular Biology, Mayo Clinic, Rochester, MN 55905, USA
[3]Department of Biochemistry and Biophysics and the Lineberger Comprehensive Cancer Center, University of North Carolina School of Medicine, Chapel Hill, NC 27599, USA
[4]Laboratory of Cell Biology, National Cancer Institute, NIH, Bethesda, MD 20892, USA
[5]Co-first author
*Correspondence: mer.georges@mayo.edu (G.M.), tatiana.kutateladze@ucdenver.edu (T.G.K.)
http://dx.doi.org/10.1016/j.str.2014.11.013

SUMMARY

p53 is dynamically regulated through various post-translational modifications (PTMs), which differentially modulate its function and stability. The dimethylated marks p53K370me2 and p53K382me2 are associated with p53 activation or stabilization and both are recognized by the tandem Tudor domain (TTD) of 53BP1, a p53 cofactor. Here we detail the molecular mechanisms for the recognition of p53K370me2 and p53K382me2 by 53BP1. The solution structures of TTD in complex with the p53K370me2 and p53K382me2 peptides show a remarkable plasticity of 53BP1 in accommodating these diverse dimethyllysine-containing sequences. We demonstrate that dimeric TTDs are capable of interacting with the two PTMs on a single p53K370me2K382me2 peptide, greatly strengthening the 53BP1-p53 interaction. Analysis of binding affinities of TTD toward methylated p53 and histones reveals strong preference of 53BP1 for p53K382me2, H4K20me2, and H3K36me2 and suggests a possible role of multivalent contacts of 53BP1 in p53 targeting to and accumulation at the sites of DNA damage.

INTRODUCTION

The tumor suppressor p53 is mutated in nearly half of all human cancers, and most of the remaining cancers are associated with decreased p53 levels or alterations in p53-mediated signaling pathways (Brosh and Rotter, 2009; Cheok et al., 2011; Levine and Oren, 2009; Muller and Vousden, 2013). p53 is a transcription factor involved in the regulation of over 100 genes essential in cell cycle control, senescence, DNA damage repair, and apoptosis (Vousden and Lane, 2007). Owing to its rapid degradation, the constitutive concentration of p53 in resting cells is maintained at a relatively low level. However, in response to DNA damage or other stress signals, p53 becomes activated and triggers growth arrest, followed by DNA damage repair or induces apoptosis if the damage cannot be repaired. Transcriptional activity, nuclear accumulation, stability, and translocation of p53 are mediated by multiple posttranslational modifications (PTMs), including phosphorylation, acetylation, methylation, ubiquitination, SUMOylation, and neddylation (Dai and Gu, 2010; Zhang et al., 2012). The PTMs are especially abundant in the C-terminal regulatory domain (CTD) of p53, which contains multiple modifiable lysine, serine, and threonine residues.

Four lysine residues, K370, K372, K373, and K382, in the p53 CTD tail are currently known to undergo methylation (Chuikov et al., 2004; Huang and Berger, 2008; Huang et al., 2006, 2007, 2010; Kachirskaia et al., 2008; Shi et al., 2007) (Figure 1A). Methylation was originally thought to influence p53 stability and function by competing for the same lysine residues that can be acetylated or ubiquitinated. It is now well established that monoubiquitination of lysines leads to p53 translocation from the nucleus to the cytoplasm, polyubiquitination targets p53 for proteasomal degradation, and acetylation increases p53 stability and occupancy at promoters of p53 target genes (Dai and Gu, 2010). Several pioneering reports have demonstrated that methylation marks in the CTD tail have an effect on transcriptional and transcription-independent functions of p53 (Chuikov et al., 2004; Huang and Berger, 2008; Huang et al., 2006, 2007, 2010; Kachirskaia et al., 2008; Shi et al., 2007). These PTMs can alter the structure, dynamics, and ability of p53 to interact with various binding partners and mediate p53 commitment to a particular pathway within a large p53-dependent signaling network.

The biological outcome of CTD methylation can lead to p53 activation or suppression, depending on the PTM position and the extent of methylation, i.e. the number of methyl groups attached to the ε-amino moiety of the lysine. Monomethylation of K372 by the lysine methyltransferase 7 (KMT7), also known as SET7/9, stabilizes p53 at chromatin and facilitates transcription of p53 target genes (Chuikov et al., 2004). In contrast, monomethylation of either K370 by KMT3C (Smyd2) or K382 by KMT5A (SET8/PR-SET7) suppresses p53 transactivation (Huang et al., 2006, 2007; Shi et al., 2007; West et al., 2010), and dimethylation of K373 by homologous KMT1C/D (G9a/Glp) also correlates with inactive p53 (Huang et al., 2010).

The dimethylated marks p53K370me2 and p53K382me2 have been identified in vivo and biochemically characterized in vitro, although methyltransferases responsible for writing these PTMs remain unknown (Huang et al., 2007; Kachirskaia

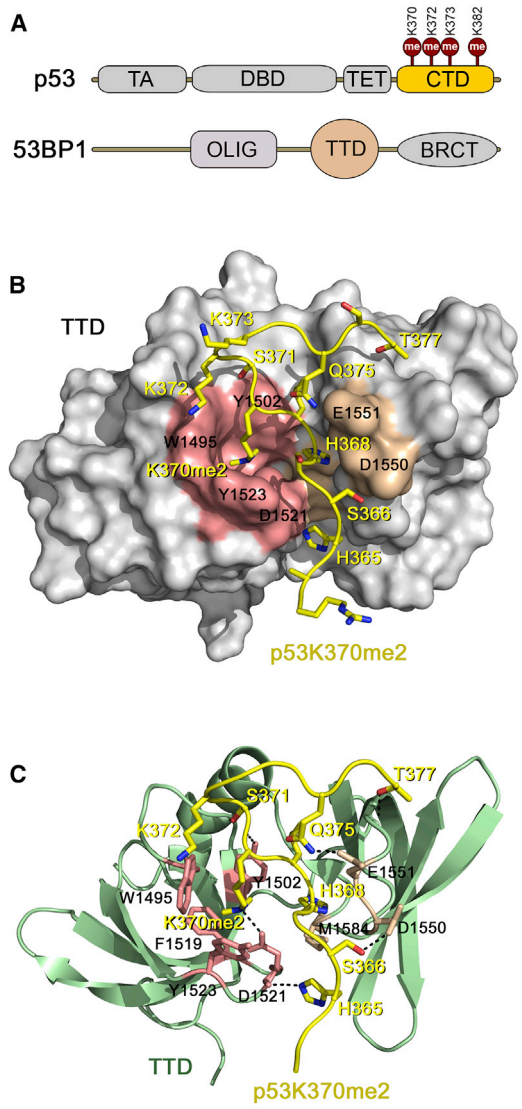

Figure 1. The Solution Structure of the Tandem Tudor Domain (TTD) of 53BP1 in Complex with a p53K370me2 Peptide

(A) Schematic representation of the domain architecture of p53 and 53BP1. BRCT, BRCA1 carboxy-terminal repeats; CTD, C-terminal domain; DBD, DNA-binding domain; Olig, oligomerization domain; TA, transactivation domain; TET, tetramerization domain; TTD, tandem Tudor domain.

(B and C) The structure of the TTD–p53K370me2 complex. TTD is depicted as a solid surface (B) and a ribbon diagram (C), with the peptide shown as a yellow ribbon. The TTD residues that form an aromatic cage around dimethylated K370 and those involved in the polar interactions with the peptide are colored salmon and wheat, respectively. p53K370me2 residues are labeled in yellow and TTD residues are labeled in black. Dashed lines represent intermolecular hydrogen bonds, see also Figures S1–S3.

et al., 2008). Cellular levels of these PTMs increase in response to DNA damage, and p53K370me2 and p53K382me2 have been simultaneously detected in stressed and unstressed cells by mass spectrometry, although it remains unclear whether these marks are present on the same p53 molecule (DeHart et al., 2014). p53K370me2 positively regulates p53 transcriptional activity and can be demethylated to a repressive p53K370me1 mark by lysine specific demethylase 1, whereas p53K382me2 is associated with p53 stability and accumulation at DNA double-strand breaks (DSBs) (Huang et al., 2007; Kachirskaia et al., 2008). Both p53K382me2 and p53K370me2 are recognized by the tandem Tudor domain (TTD) of p53-binding protein 1 (53BP1) (Figure 1A) (Huang et al., 2007; Kachirskaia et al., 2008). Interaction of the TTD module with p53K382me2 plays a role in p53 stabilization at DSBs and binding to p53K370me2 is essential for p53 transactivation upon DNA damage (Huang et al., 2007; Kachirskaia et al., 2008). 53BP1 is a key DNA damage response mediator and a coactivator of p53, which also recognizes methylated histones, H4K20me2 particularly, as well as dimethylated at K810 retinoblastoma protein and DNA (Botuyan et al., 2006; Carr et al., 2014; Charier et al., 2004; Huyen et al., 2004; Kim et al., 2006). Recent studies have shown that the association of 53BP1 TTD with H4K20me2 is necessary but not sufficient to rapidly recruit 53BP1 to damaged DNA. Such recruitment requires oligomerization of 53BP1 through its oligomerization domain, located upstream of the TTD (Fradet-Turcotte et al., 2013; Ward et al., 2006; Zgheib et al., 2009), and ubiquitination of histone H2A (Fradet-Turcotte et al., 2013). The pairing of TTDs via 53BP1 oligomerization raises the possibility for a mechanistic and functional crosstalk between multiple dimethyllysine substrates, including PTMs on p53 and histones.

Here we describe the molecular basis for binding of the 53BP1 TTD module to p53K370me2 and p53K382me2. Nuclear magnetic resonance (NMR) structures of the complexes reveal a remarkable plasticity of 53BP1 in accommodating these diverse dimethyllysine-containing sequences. Analyses of binding affinities and specificities indicate that 53BP1 can simultaneously recognize dual K370me2/K382me2 marks on a single p53 substrate and suggest a model for rapid accumulation of p53 at DSBs that involves multiple interactions of oligomeric 53BP1 with p53, H4K20me2, and H3K36me2.

RESULTS AND DISCUSSION

p53K370me2 Is Bound in a Deep Cleft of 53BP1 TTD

To elucidate the mechanism for the recognition of p53K370me2, we determined the solution structure of 53BP1 TTD in complex with a p53K370me2 peptide (residues R363–T377 of p53). We previously attempted to crystallize the p53K370me2-TTD complex (Roy et al., 2010); however, electron density seen only for the K370me2 residue of the peptide precluded analysis of the binding mechanism and prompted us to obtain the structure using NMR spectroscopy. The solution structure of the p53K370me2-bound TTD shows a canonical fold of the domain, consisting of the tandem five-stranded β barrels linked by a C-terminal α helix (Figures 1B and 1C; Table 1; Figures S1 and S2 available online). The NMR assemble also reveals an extensive protein–peptide interface of 707 ± 43 Å^2.

The amino-terminal residues of the p53 peptide, H365-S371, occupy a long, deep cleft at the Tudor1–Tudor2 border (Figure S1). From a total of 68 intermolecular nuclear Overhauser enhancements (NOEs), 66 signals involve these residues of p53. The centrally positioned p53 L369 lies in a hydrophobic cavity created by the Y1500, L1547, Y1520, M1554, and I1587 residues of the protein (Figure S2). L369 contributes 31 intermolecular NOEs (13 with Y1502, 6 with L1547, 5 with Y1500, 3 with

Table 1. NMR and Refinement Statistics

NMR Distance and Dihedral Restraints	53BP1 TTD–p53K370me2	53BP1 TTD–p53K382me2
Distance Restraints		
Total NOE	4,243	4,099
Intraresidue	889	848
Interresidue	3,286	3,212
Sequential ($\|i-j\|=1$)	850	822
Medium range ($\|i-j\|<5$)	722	697
Long range($\|i-j\|>4$)	1,714	1,693
Intermolecular	68	39
Hydrogen bonds	65	65
Total Dihedral Angle Restraints	226	226
ϕ	76	78
ψ	77	77
$\chi 1$	73	71
Additional Distance Constraints		
Crystallography-based restraints[a]	15	15
Structure Statistics		
Violations (mean ± SD)		
Distance constraints (Å)	0.10 ± 0.02	0.08 ± 0.04
Dihedral angle constraints (°)	2.67 ± 0.96	1.82 ± 1.02
Maximum dihedral angle violation (°)	4.46	3.77
Maximum distance restraint violation (Å)	0.16	0.20
Deviations from Idealized Geometry		
Bond lengths (Å)	0.0080 ± 0.0001	0.0081 ± 0.0001
Bond angles (°)	2.08 ± 0.02	2.83 ± 0.24
Impropers (°)	0.23 ± 0.01	1.67 ± 0.33
Average Pairwise Root-Mean-Square Deviation (Å)[b]		
Heavy	0.94 ± 0.09	1.11 ± 0.12
Backbone	0.50 ± 0.07	0.64 ± 0.11

[a]Additional distance restraints involving K370me2 and K382me2 were derived from crystal structures of these complexes.
[b]Calculated from residues 1488–1603 of 53BP1, residues 365–371 of p53K370me2, and residues 379–385 of p53K382me2.

M1584, 2 with I1587, 1 with E1549, and 1 with E1551). In the crystal structure of p53K370me2-bound TTD, the side chain of K370me2 inserts in the aromatic cage formed by the four aromatic residues, W1495, Y1502, F1519, and Y1523, and a negatively charged aspartate, D1521 (Roy et al., 2010). The aromatic moieties make favorable hydrophobic and cation-π contacts with the dimethylammonium group of p53 K370, and the carboxylate of D1521 forms a hydrogen bond with the only amino proton and a salt bridge with the ion. Two NOEs detected between K370me2 and the aromatic cage residues and the chemical shift perturbations (CSPs) at the 53BP1–p53K370me2 interface are fully consistent with K370me2 occupying the aromatic cage in the solution structure (see Experimental Procedures; Figure S2B).

The side chains of p53 H368 and S371 are well restrained by 15 and 8 intermolecular NOEs, respectively. The tandem lysine residues p53 K372 and p53 K373 are solvent exposed and the carboxyl-terminal residues p53 G374–T377 are relatively flexible (Figure S2). Overall, a number of polar, electrostatic, and hydrophobic interactions of the TTD with p53K370me2 unambiguously position the p53 peptide in such a manner that the N terminus of the peptide is bound near the β3–β4 loop of Tudor1 and the β6–β7 loop of Tudor2, whereas the C terminus of p53 is oriented toward the α helix of the TTD.

We examined the contribution of the potential intermolecular hydrogen bonding and hydrophobic contacts to complex formation by comparing CSPs in $^{1}H,^{15}N$ heteronuclear single quantum coherence (HSQC) spectra of ^{15}N-labeled TTD bound to p53K_C370me2 peptides. In these peptides, K370 was replaced with a dimethyllysine analog (*N*-dimethylated aminoethylcysteine, K_C370me2), whereas other residues were individually substituted with a flexible glycine (Figure S3). Alterations in CSPs induced by p53H365GK_C370me2, p53H368GK_C370me2, and p53L369GK_C370me2 peptides confirmed the important role of the buried H365, H368, and L369 residues for the interaction with TTD. However, the solvent-exposed K372 and K373 appear to be dispensable, as p53K_C370me2K372G and p53K_C370me2K373G peptides caused the same CSPs as the wild-type p53K_C382me2 peptide.

p53K382me2 Is Bound in a U-shape Conformation

To obtain molecular insight into the recognition of p53K382me2, we determined the solution structure of 53BP1 TTD bound to the p53K382me2 peptide (residues S376–T387 of p53) (Table 1). The NMR assemble shows a large protein–peptide interface of 678 ± 60 $Å^2$. Unexpectedly, we found that in the complex, the p53K382me2 peptide adopts a U-shape conformation and binds in the orientation that is opposite to the orientation of the p53K370me2 peptide (Figure 2). In contrast to p53K370me2, the N terminus of the p53K382me2 peptide is positioned near the second β barrel, and we were unable to superimpose the structures of the two peptides in the bound states.

Much like dimethylated K370 of the p53K370me2 peptide, dimethylated K382 of p53K382me2 lies in the aromatic cage of the TTD; however, the rest of the peptide residues are bound differently (Figure 2A). The carboxyl group of TTD E1551 forms a salt bridge with the guanidino group of p53 R379. Four intermolecular NOEs position p53 H380 in the vicinity of Y1500, F1553, L1547, and I1587. The conformation of p53 K381 is fixed through four NOEs to Y1500 and three NOEs to Y1502. The side chains of L383 and F385 contact a hydrophobic groove formed by the Y1502, L1547, M1584, and I1587 residues of the TTD. Fifteen NOEs are seen between these TTD residues and p53 L383, whereas the aromatic ring of F385 is constrained via seven intermolecular NOEs with the TTD residues L1547, I1587, M1584, and Y1523 (Figure S2). The side chains of p53 M384 and p53 K386 appear to be unrestrained.

Comparative analysis of CSPs produced in the TTD by glycine mutants of p53K_C382me2 peptide revealed the important role of the p53 residues adjacent to the dimethyllysine, such as R379, H380, K381, L383, and F385 (Figure S3). NMR titration experiments showed that among eight mutant peptides tested, p53R379GK_C382me2, p53H380GK_C382me2,

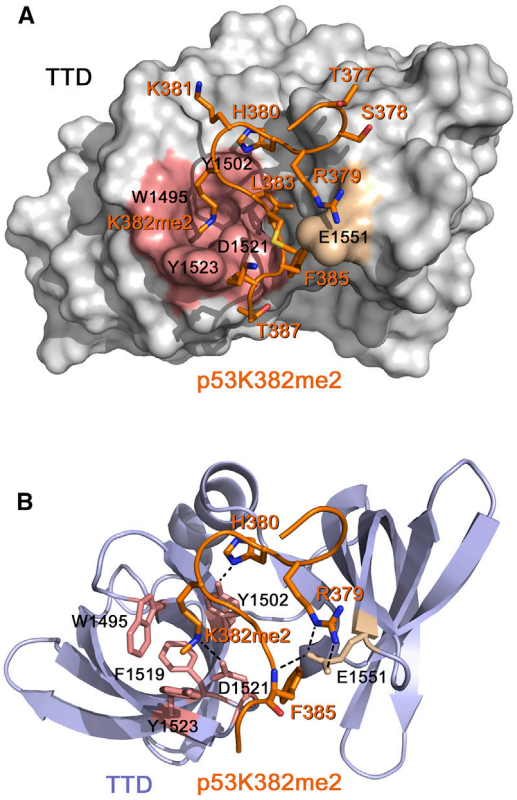

Figure 2. The Solution Structure of the 53BP1 TTD in Complex with a p53K382me2 Peptide

(A and B) TTD is depicted as a solid surface (A) and a ribbon diagram (B), with the peptide shown as an orange ribbon. The TTD residues that form an aromatic cage around dimethylated K382 and those involved in the polar interactions with the peptide are colored salmon and wheat, respectively. p53K382me2 residues are labeled in orange and TTD residues are labeled in black. Dashed lines represent intermolecular hydrogen bonds, see also Figures S2 and S3.

p53K381GK$_C$382me2, p53K$_C$382me2L383G, and p53K$_C$382me2F385G altered the pattern of CSPs caused by the wild-type p53K$_C$382me2 peptide, indicating that the R379, H380, K381, L383, and F385 residues significantly contribute to the interaction with TTD. These data were in agreement with previous findings that the replacement of H380 and K381 with an alanine reduces binding of the TTD ~16-fold and 11-fold, respectively (Roy et al., 2010).

An alignment of methyllysine-containing p53 CTD and histone tail sequences shows a high degree of similarity between p53K382me2 and H4K20me2, which may imply a comparable binding mechanism (Figure 3A). The overlaid NMR structures of the peptides derived from the TTD-p53K382me2 and TTD-H4K20me2 (Tang et al., 2013) complexes demonstrate that although both peptides are oriented in a similar manner, the overall binding modes differ (Figure 3B). Our results point to a high plasticity of 53BP1 TTD in accommodating the dimethyllysine substrates. Furthermore, such an intricate recognition of each of the p53K370me2, p53K382me2, and H4K20me2 sequences suggests that the TTD can distinguish between dimethyllysine marks (see below). It also suggests a possibility of generating distinct mutations in 53BP1 TTD that impair binding to a particular dimethyllysine ligand. Interestingly, the hybrid Tudor domains of JMJD2A (KDM4A) have previously been found to recognize histone H3K4me3 and H4K20me3 peptides using different binding mechanisms (Lee et al., 2008).

We note that the same p53 peptide acetylated at K382 (p53K382ac) has been shown to bind in a remarkably similar U-shape conformation to a bromodomain of CBP, a structurally unrelated module (Mujtaba et al., 2004), implying that the p53K382 region may prefer this bound-state conformation, irrespective of the nature of PTM on K382 (Figure 3C).

The First but not the Second β Barrel of 53BP1 TTD Is Functional

A thorough mass spectrometry analysis of PTMs on p53 has shown the coexistence of p53K370me2 and p53K382me2 in human foreskin fibroblasts treated with a DNA damage-inducing agent, etoposide, as well as in the untreated cells (DeHart et al., 2014). Although it remains unclear if both marks are present on the same p53 molecule, previous observations that cellular levels of these PTMs increase in response to DNA damage suggest that they may (Huang et al., 2007; Kachirskaia et al., 2008). Furthermore, the two sequential single Tudor domains of PHF20 have been shown to form a dimer, which could associate with the p53 CTD dimethylated at K370 and K382 (Cui et al., 2012). We examined the ability of the 53BP1 TTD to bivalently interact with p53K370me2K382me2. Structural analysis of the 53BP1 complexes reveals that the TTD folds into two almost identical β barrels, with the dimethyllysine substrate being bound in the aromatic cage of the first β barrel. As the second β barrel also contains a cluster of aromatic residues, we tested whether each β barrel is capable of accommodating a dimethyllysine PTM. Of note, the distance (~20 Å) between the aromatic patches of the TTD is ideal for the interaction with p53K370me2K382me2 (Figures 4A and 4B). We generated the p53K370me2K382me2 peptide using solid-phase peptide synthesis and tested it in NMR and fluorescence spectroscopy assays.

Titration of the p53K370me2K382me2 peptide into ^{15}N-labeled 53BP1 TTD resulted in large CSPs in ^{1}H,^{15}N HSQC spectra of the protein (Figure 4C). Plotting CSPs for each TTD residue and mapping the most significant changes onto the TTD structure revealed that the aromatic cage of the first β barrel of TTD is substantially perturbed (Figures 4D and 4E). However, the aromatic patch of the second β barrel was essentially unaffected, implying that only the first but not the second β barrel of the TTD is functional (Figures 4C–4E). This is in striking contrast to the homodimeric Tudor domains of PHF20, each of which associates with dimethylated p53 (Cui et al., 2012).

Notably, the binding pocket of the second β barrel of 53BP1 TTD is basic in nature, whereas the binding pocket of the first β barrel is acidic (Figure S4). Electrostatic repulsion of a positively charged methyllysine may contribute to the inability of the second β barrel to accommodate this PTM. The intermediate exchange regime on the NMR chemical shift timescale for the interaction of the TTD with p53K370me2K382me2 indicated a stronger binding in comparison with binding to the singly modified peptides, due to an increase in local concentration of the dimethyllysine ligand in p53K370me2K382me2 (Figure 4C).

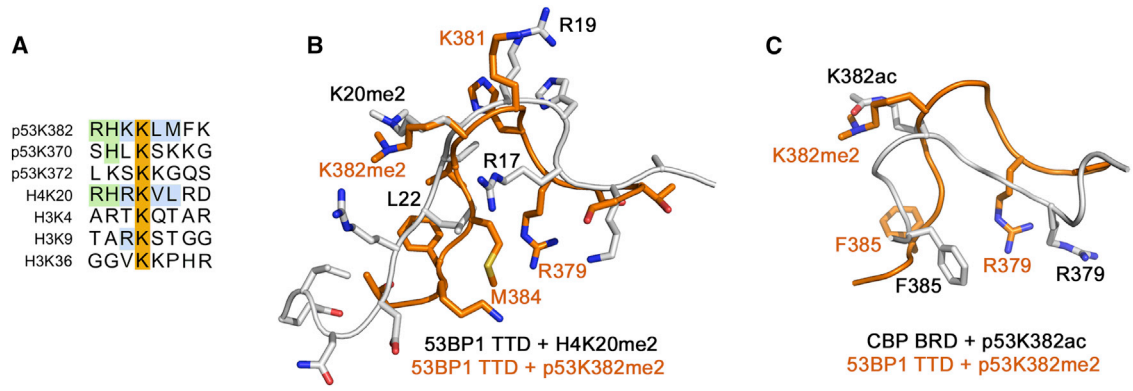

Figure 3. Recognition of the Dimethyllysine Sequences by the 53BP1 TTD

(A) Alignment of the p53 and histone H3 and H4 sequences with dimethylated lysine residues highlighted in orange. Moderately and weakly conserved residues are colored green and blue.

(B) Structural overlay of the p53K382me2 peptide (orange) bound to TTD and the H4K20me2 peptide (gray) bound to TTD (PDB 2LVM). TTD is not shown.

(C) Structural overlay of the p53K382me2 peptide (orange) bound to TTD and the p53K382ac peptide (gray) bound to a bromodomain of CBP (PDB 1JSP). TTD and the bromodomain are not shown.

Thus, we concluded that although the 53BP1 TTD binds better to the proximate methylation PTMs on p53, it utilizes only the aromatic cage of the first β barrel to do so.

Dimeric TTDs Bind Robustly to p53K370me2K382me2

Oligomerization of 53BP1 links multiple TTDs, making it possible for 53BP1 to simultaneously associate with several methyllysine targets. To mimic the oligomerization-mediated pairing of TTDs and to examine whether the linked modules are capable of concurrent binding to p53K370me2K382me2, we generated a longer 53BP1 construct, consisting of residues 1481–1603 and incorporated a cysteine residue at the N terminus. In this construct, native cysteine residues 1525 and 1535 were mutated to alanines. The purified ^{15}N-labeled protein was chemically crosslinked to form an N terminus to N terminus homodimer (CL-TTD) using bismaleimide and then separated from the monomeric form by chromatography (Figure 5A; Figure S5). A comparison of the ^{1}H,^{15}N HSQC spectrum of CL-TTD with that of TTD revealed several additional peaks, likely belonging to the linker residues, and a few resonance changes, most of which were clustered around the points of alanine mutations of the native cysteine residues (Figure 5B). The lack of significant differences in chemical shifts and limited changes in the line widths suggested a full flexibility of the crosslinked domains.

Addition of the singly modified p53K382me2 peptide to uniformly ^{15}N-labeled CL-TTD caused substantial chemical shift changes in the protein (Figure 5C). The pattern of CSPs indicated that both crosslinked domains bind to the methylated peptide in a manner similar to the binding of a single TTD. However, upon titration of the doubly methylated p53K370me2K382me2 peptide, many peaks in the ^{1}H,^{15}N HSQC spectra of CL-TTD broadened and disappeared (Figure 5C, third panel). Particularly, the CL-TTD residues located in and around the methyllysine-binding pocket in the first β barrel showed a significant decrease in intensity (Figure S5). The overall decrease in cross-peak intensity implied a decrease in flexibility of the two TTDs and/or the formation of a larger, slow tumbling complex, and thus suggested that the CL-TTD associates with both PTMs on a single p53K370me2K382me2 peptide. In agreement, binding of an equimolar mixture of the p53K370me2 and p53K382me2 peptides to the CL-TTD failed to produce a large complex, as no significant change in resonance intensities was observed (Figure 5C, second panel).

The ability of CL-TTD to bivalently associate with the p53K370me2K382me2 peptide was substantiated through measuring binding affinities. Analysis of the binding curves of CL-TTD in fluorescence assays required a two-site-binding model and yielded K_d values of 0.1 μM and 17 μM, indicating that both linked TTDs were involved in the interaction with the peptide (Figure 6A; Figure S5). The increase in affinity of the linked TTDs compared with binding affinities of the individual TTDs is likely entropically driven, as both TTDs and dimethylated PTMs are prealigned for the interaction. Furthermore, the dimeric glutathione *S*-transferase (GST)-fused TTD, in which the two TTD molecules are ideally oriented for concurring interactions with the double PTMs, bound to the p53K370me 2K382me2 peptide stronger (K_d values of 0.01 μM and 2.6 μM) (Figure S5E).

Models for the Bivalent Interactions of 53BP1 TTDs

Generally, oligo(di)merization of 53BP1 can promote binding of the TTD either to multiple dimethyllysine marks on a single peptide (in *cis*), or to dimethyllysine PTMs on multiple proteins (in *trans*). Modeling of the p53K370me2-TTD and p53K382me2-TTD complexes suggests that p53K370me2K382me2 can hold a pair of TTDs in a sequential manner, with the avidity effect enhancing this association (Figure 6B).

Alternatively, the linked TTDs could bridge dimethylated p53 with dimethylated histone tails. It was previously reported that 53BP1 TTD binds to H4K20me2 (Botuyan et al., 2006) and weakly associates with some other dimethylated histones (Botuyan et al., 2006; Huyen et al., 2004; Kim et al., 2006); however, a comprehensive analysis of the TTD substrates has not been performed. To establish the 53BP1 TTD specificity, we designed an extensive library of peptides containing known PTMs on core and variant histones and on the p53 CTD (Table S1) and

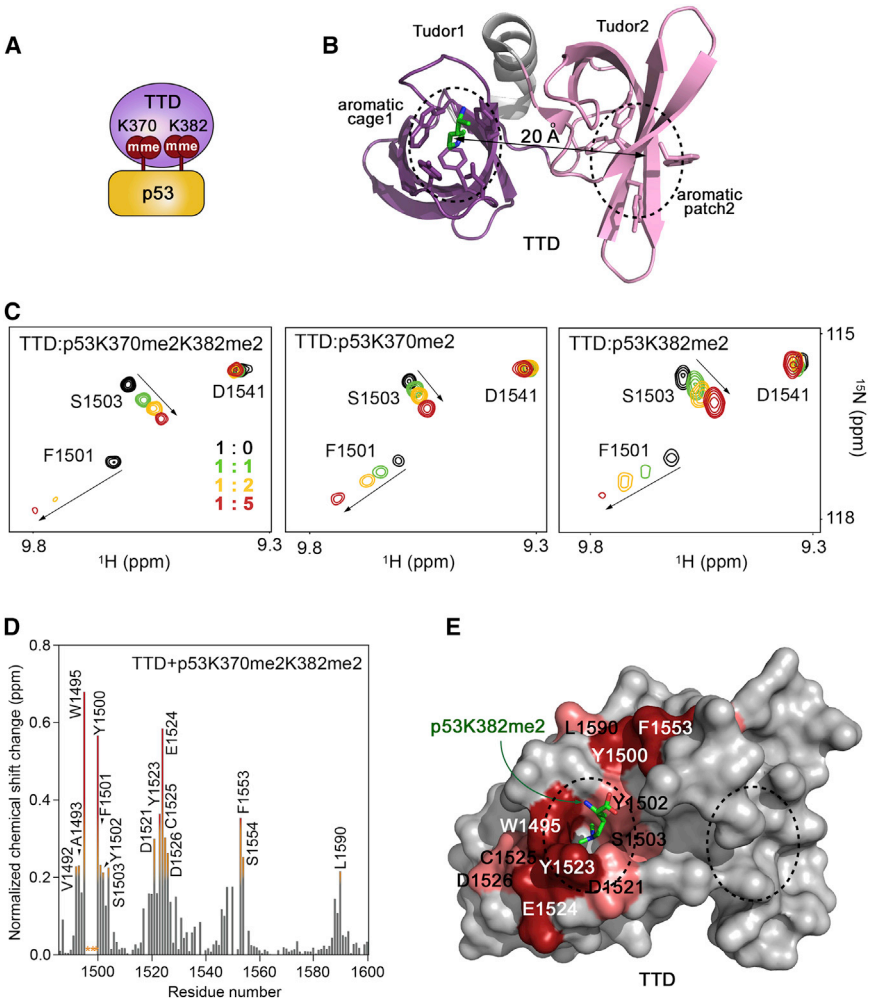

Figure 4. The First β Barrel of the 53BP1 TTD Is Functional

(A) Possible bivalent interactions of TTD.

(B) The 53BP1 TTD is shown as a ribbon diagram, with the dimethyllysine (green) bound in the aromatic cage of the first β barrel. The aromatic pockets of Tudor1 and Tudor2 are outlined.

(C) Superimposed $^{1}H,^{15}N$ HSQC spectra of TTD collected upon titration with the indicated p53 peptides. Spectra are color coded according to the protein/peptide molar ratio (see inset).

(D) The normalized chemical shift changes observed in $^{1}H,^{15}N$ HSQC spectra of TTD upon titration with p53K370me2K382me2 peptide as a function of residue.

Residues showing large chemical shift differences are mapped onto the structure of TTD in (E), see also Figure S4.

examined binding of GST-tagged 53BP1 TTD (Figure 6C). Screening GST-TTD against the library showed that among the p53 peptides tested, the protein recognized primarily p53K382me2, and to a lesser degree p53K370me2. These data corroborated well the K_d values of 0.9 μM and 20 μM, measured for the interactions of TTD with p53K382me2 and p53K370me2, respectively (Roy et al., 2010) (Figure 6A). The peptide library screening also confirmed a robust binding to histone H4K20me2 (K_d = 1.3 μM) (Botuyan et al., 2006; Roy et al., 2010) (Figure 6C). Unexpectedly, we detected a strong interaction of the 53BP1 TTD with H3K36me2. Binding to H3K18me2 was weaker, and much weaker associations with other dimethyllysine-containing histone peptides, including H3K79me2, were observed. To further verify the peptide library data, we measured the binding affinity of the TTD for H3K36me2 using tryptophan fluorescence. The K_d value was found to be 1.5 μM, which is comparable with the affinity of TTD for p53K382me2 and H4K20me2 (Figure 6A). The pattern of CSPs in $^{1}H,^{15}N$ HSQC spectra of the TTD induced by H3K36me2 peptide suggested that dimethylated K36 occupies the aromatic cage (Figure S6). These results demonstrate that the 53BP1 TTD module has a strong preference toward the p53K382me2, H4K20me2, and H3K36me2 sequences.

Concluding Remarks

The discovery of numerous PTMs on p53 reveals a complex signaling network that resembles the histone code phenomenon (Strahl and Allis, 2000), yet the biological significance of the p53 methyllysine marks and their relationship with histone PTMs remain largely unexplored. In this study, we determined the molecular mechanisms for the recognition of p53K382me2 and p53K370me2 by the TTD module of a p53 coactivator, 53BP1. 53BP1 is a mediator and effector of the DSB response that plays a central role in DNA damage repair (Panier and Boulton, 2014). We also found that the 53BP1 TTD has a strong preference for p53K382me2, H4K20me2, and H3K36me2, and this selectivity suggests a possible role of multivalent contacts in 53BP1 localization and activity.

DNA damage triggers an acute mobilization of 53BP1 to DSB sites, and both oligomerization of 53BP1 and binding of the TTD to H4K20me2 are required for the efficient recruitment of 53BP1 (Botuyan et al., 2006; Fernandez-Capetillo et al., 2002; Fradet-Turcotte et al., 2013; Huyen et al., 2004; Kachirskaia et al., 2008; Rappold et al., 2001; Roy et al., 2010; Zgheib et al., 2009). However, H4K20me2 is a highly abundant PTM, which is ubiquitously present in the majority (>80%) of nucleosomes in mammalian cells (Panier and Boulton, 2014). H4K20me2 is generated independently of DNA damage and therefore cannot instigate a specific focal recruitment of 53BP1 to DNA lesions (Panier and Boulton, 2014), whereas H3K36me2 can. The H3K36me2 levels increase considerably at the DSB sites following DNA damage (Fnu et al., 2011; Jha and Strahl, 2014; Pai et al., 2014). H3K36me2 recruits and stabilizes components of the DNA repair machinery, and installation of this PTM has been shown to be a major immediate methylation event at DSBs, which also correlates with the DNA repair efficiency (Fnu et al., 2011; Musselman et al., 2012a). DNA damage raises p53K382me2 levels as well (Kachirskaia et al., 2008).

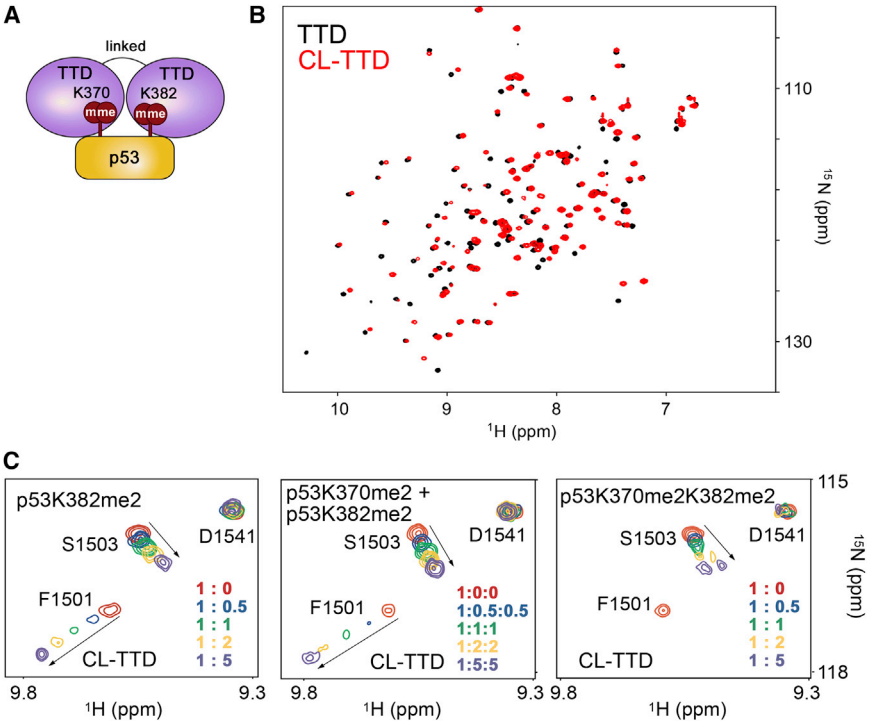

Figure 5. Crosslinked TTDs Bind to p53K370me2K382me2

(A) Possible oligomerization-mediated bivalent interactions of TTD.

(B) An overlay of $^{1}H,^{15}N$ HSQC spectra of TTD (black) and CL-TTD (red).

(C) Superimposed $^{1}H,^{15}N$ HSQC spectra of CL-TTD collected upon titration with the indicated p53 peptides, see also Figure S5.

Accordingly, oligomerized 53BP1 could concurrently associate with p53K382me2 and H3K36me2, recruiting p53 to DSBs. Binding of the TTD to the abundant H4K20me2 and the association of a short neighboring region with H2A ubiquitinated at K15 (Fradet-Turcotte et al., 2013) can stabilize 53BP1 at damaged DNA, contributing to anchoring or retention of 53BP1. Other methyllysine marks, including p53K370me2, which is also generated in response to DNA damage (Huang et al., 2007), may aid in the p53-53BP1-chromatin assembly by enhancing avidity of oligomeric 53BP1. This mechanism of rapid accumulation and stabilization of 53BP1/p53 could be critical in the early response to DNA damage; however, further studies will be necessary to fully explore it.

EXPERIMENTAL PROCEDURES

Protein and Peptide Expression, Purification, and Crosslinking

The wild-type TTD of human 53BP1 (residues 1484–1603 and 1481–1603) was expressed and purified as reported previously (Botuyan et al., 2006; Roy et al., 2010). The C1525A/C1535A mutant of the 1481–1603 TTD was generated by site-directed mutagenesis using the Stratagene QuikChange Mutagenesis protocol. To generate a crosslinked TTD, a Cys residue was added to the N terminus of the C1525A/C1535A construct. The TTD was crosslinked at room temperature for 2 hr in PBS using bismaleimidoethane (Thermo Scientific Pierce). Monomer and crosslinked homodimer were separated using a Superdex 75 10/300 GL Tricorn column (GE Life Sciences).

The p53K370me2 (residues 363–377) and p53K382me2 (residues 376–387) peptides were chemically synthesized and purified by reversed-phase high-performance liquid chromatography. To allow ^{13}C and ^{15}N isotope enrichment for NMR spectroscopy experiments, the p53 peptides were also produced in *Escherichia coli* as a fusion to an N-terminal GB1–hexahistidine tag cleavable by TEV protease, chemically modified to install a dimethylated lysine analog (K_C370me2 or K_C382me2 with and without ^{13}C enrichment of the two methyl groups) and purified by size exclusion and reversed-phase chromatography, as reported previously (Cui et al., 2009). The recombinant peptides include three N-terminal expression vector-encoded residues (Gly-His-Met). The p53K370me2K382me2 peptide (residues S366–K386) was synthesized by 9-fluorenylmethoxycarbonyl solid-phase peptide synthesis using an Applied Biosystem 431A peptide synthesizer, as described (Roy et al., 2010).

Solution Structures of the TTD-p53K370me2 and TTD-p53K382me2 Complexes

The NMR experiments were recorded at 298 K using a Bruker Avance 700 MHz spectrometer equipped with a cryoprobe. Protein samples were made in 25 mM sodium phosphate (pH 7.5), 90% H_2O/10% D_2O or 100% D_2O and 1.5 mM NaN_3. Different samples were prepared for complex resonance assignments and structure determination. These are 2 mM $^{13}C/^{15}N$-labeled 53BP1 TTD and 6 mM nonlabeled p53K370me2 (or p53K382me2), and 2 mM $^{13}C/^{15}N$-labeled p53K_C370me2 and 5 mM nonlabeled 53BP1 TTD. Because of difficulties producing the p53Kc382me2 peptide from expression in *E. coli*, a low concentration complex of 0.5 mM $^{13}C/^{15}N$-labeled p53K_C382me2 and 2 mM nonlabeled 53BP1 TTD was prepared and used only to facilitate resonance assignment. No intermolecular NOEs were measured from this sample. A combination of 2D ^{1}H-^{15}N HSQC, ^{1}H-^{13}C HSQC and 3D HNCA, HNCACB, CBCA(CO)NH, HNCO, HN(CA)CO, (H)CC(CO)NH, H(CC)(CO)NH, HBHA(CO)NH, ^{15}N-TOCSY-HSQC, and (H)CCH-TOCSY experiments were used for 53BP1 TTD backbone and side-chain assignments. 2D ^{1}H-^{13}C HSQC and 3D ^{13}C-NOESY HSQC optimized for aromatic resonances as well as 2D (HB) CB(CGCD)HD were collected to assign 53BP1 TTD aromatic ring resonances. 2D ^{1}H-^{13}C HSQC and 3D (H)CCH-TOCSY and ^{13}C-NOESY HSQC were recorded to assign p53K_C370me2 resonances. $^{13}C/^{15}N$ double-filtered ^{13}C-edited 3D NOESY HSQC spectra (Zwahlen et al., 1997) were recorded to identify intermolecular NOEs. The NOE signals were assigned through several iterations of CYANA (version 2.1) (Güntert, 2004) and SANE (Duggan et al., 2001) calculations. For the initial structure calculations, we used only intermolecular NOEs corresponding to easily identifiable signals from 53BP1 TTD and the p53 peptides, such as NOEs involving the methyl groups of 53BP1 TTD and p53 (Mer et al., 2000). Through multiple iterations, we were able to manually assign a total of 68 intermolecular NOEs for the 53BP1 TTD–p53K370me2complex. For the 53BP1 TTD–p53K382me2 complex, a total of 39 intermolecular NOEs were assigned. Because of exchange broadening and signal disappearance for residues in the 53BP1 aromatic cage, only two NOEs involving p53 residue K370me2 were detected (K370 HB# and 53BP1 Y1502 HD#) and none for p53K382me2. For the structure calculation, we therefore included 15 distance restraints derived from the crystal structures of 53BP1 TTD in complex with p53K370me2 and p53K382me2 (Roy et al., 2010) to position the side chain of K370me2 and K382me2. The NMR data were processed using NMRPipe (Delaglio et al., 1995) and analyzed using NMRView (Johnson and Blevins, 1994).

The interproton distances derived from signal integration of the NOESY spectra were classified into five categories, corresponding to a lower

A

	Peptide	Kd (μM)
CL-TTD	p53K370me2K382me2	0.11 +/- 0.08 (site 1) 17 +/- 4 (site 2)
	p53K382me2	1.1 +/- 0.1

	Peptide	Kd (μM)
TTD	p53K382me2	0.9 +/- 0.4*
	p53K370me2	20 +/- 4*
	H4K20me2	1.3 +/- 0.2*
	H3K36me2	1.5 +/- 0.4

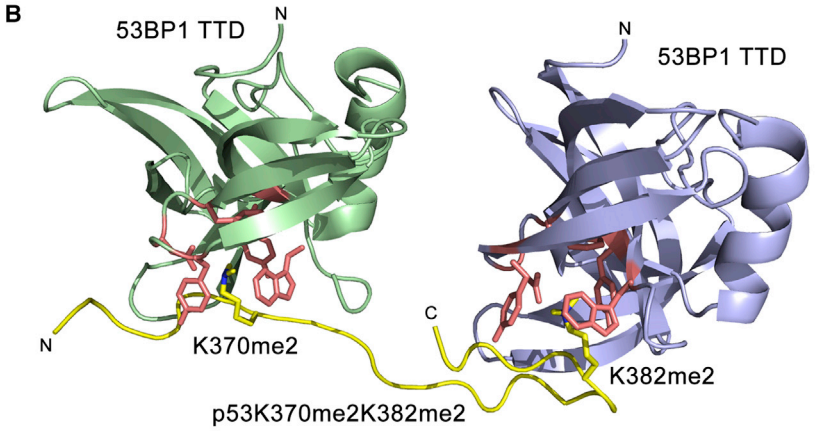

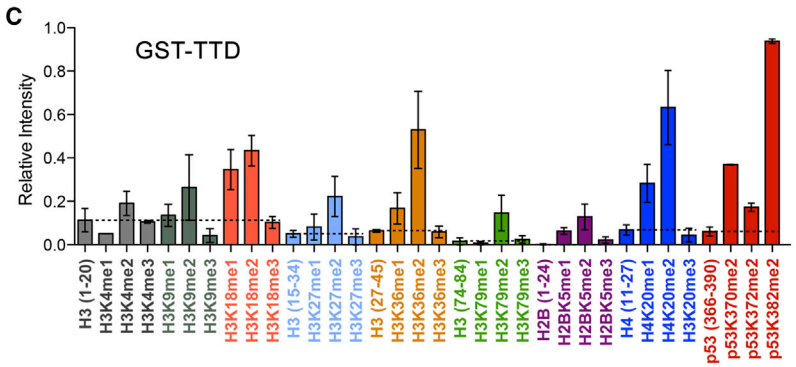

Figure 6. Bivalent Interactions of the 53BP1 TTDs

(A) Affinities of TTD and CL-TTD as determined by tryptophan fluorescence spectroscopy. *Taken from (Roy et al., 2010).

(B) Modeling the bivalent association of CL-TTD with p53K370me2K382me2 using the structures of TTD in complex with p53K382me2 and p53K370me2 and the structure of p53 peptide.

(C) Effects of the indicated PTMs on the binding of the 53BP1 TTD to histone and p53 peptides. Results of four arrays are presented as normalized mean intensities. Error bars represent SEM from pooled averages. Dotted lines demarcate groups of peptides with conserved sequence, see also Figure S6 and Table S1.

NMR Titration Experiments

^{1}H,^{15}N HSQC spectra were collected at 298 K on 0.1–0.2 mM uniformly ^{15}N-labeled TTD or CL-TTD on a Varian INOVA 600-MHz spectrometer equipped with a cryogenic probe. Binding was characterized by monitoring chemical shift changes as differently modified p53 peptides or H3K36me2 peptide were added stepwise.

Fluorescence Spectroscopy

Tryptophan fluorescence measurements were recorded on a Fluoromax-3 spectrofluorometer (HORIBA) at room temperature. The samples containing 0.2–0.5 μM CL-TTD, GST-TTD, or TTD and progressively increasing concentrations of the dimethylated p53 or histone peptides were excited at 295 nm. Emission spectra were recorded from 305 to 405 nm with a 0.5 nm step size and a 1 s integration time, averaged over three scans. The K_d values were determined as described (Musselman et al., 2009, 2012b). The K_d values were averaged over three separate experiments, with the error calculated as the SD between runs.

Peptide Microarray

Peptide synthesis and validation, microarray fabrication, effector protein hybridization and detection, and data analysis were performed as previously described (Gatchalian et al., 2013).

distance limit of 1.8 Å and upper limits of 2.8, 3.5, 4.5, 5.5, and 7.5 Å. The upper limit of 7.5 Å was used only for very weak signals, which could be due to spin diffusion. Distance restraints corresponding to hydrogen bonds identified from $^{1}H/^{2}D$ exchange experiments were also included with upper limits of 3.2 Å and 2.2 Å for N–O and HN–O, respectively. Dihedral angle restraints φ and ψ were derived from TALOS (Cornilescu et al., 1999) and chemical shift index (Wishart and Sykes, 1994) analysis and included in the calculations with a tolerance of ± 30°. χ^{1} angle restraints were based on NOE intensity analysis and, likewise, were included in the calculations, with a tolerance of ±30°.

Two hundred structures were calculated using CYANA, of which the 100 structures with lowest energies were refined by simulated annealing using AMBER (Case et al., 2005), with inclusion of the generalized Born solvation model (Tsui and Case, 2000). The force constants were 20 kcal mol^{-1} $Å^{-2}$ for NOE-derived distance restraints, 40 kcal mol^{-1} $Å^{-2}$ for hydrogen bond-derived distance restraints, 50 kcal mol^{-1} rad^{-2} for dihedral angle restraints, 100 kcal mol^{-1} rad^{-2} for chirality restraints, and 150 kcal mol^{-1} rad^{-2} for omega angle restraints. The 20 structures with the lowest AMBER energies and lowest dihedral angle violations were retained for the final analysis. The quality of the final structures was assessed using PROCHECK-NMR. The structural statistics are provided in Table 1.

ACCESSION NUMBERS

Atomic coordinates for the structures have been deposited in the Protein Data Bank (PDB) under accession codes 2MWO and 2MWP for 53BP1-TTD-p53K370me2 and 53BP1-TTD-p53K382me2, respectively.

SUPPLEMENTAL INFORMATION

Supplemental Information includes six figures and one table and can be found with this article online at http://dx.doi.org/10.1016/j.str.2014.11.013.

AUTHOR CONTRIBUTIONS

Q.T., G.C., G.M., and T.G.K. designed the study. Q.T., G.C., M.V.B., and S.B.R. performed experiments and together with R.H., C.A.M., N.S., E.A., B.D.S., G.M., and T.G.K. analyzed the data. T.G.K. wrote the manuscript with input from all authors.

ACKNOWLEDGMENTS

This research is supported by grants from the NIH, GM101664 (T.G.K.), CA132878 (G.M.), GM110058 (B.D.S.) and CA181343 (S.B.R.). G.M. acknowledges partial support from the Mayo Clinic SPORE NCI grants P50CA116201 and P50CA108961. This research is also supported in part by the Intramural Research Program of the Center for Cancer Research, National Cancer Institute, NIH (EA).

Received: June 30, 2014
Revised: November 11, 2014
Accepted: November 13, 2014
Published: January 8, 2015

REFERENCES

Botuyan, M.V., Lee, J., Ward, I.M., Kim, J.E., Thompson, J.R., Chen, J., and Mer, G. (2006). Structural basis for the methylation state-specific recognition of histone H4-K20 by 53BP1 and Crb2 in DNA repair. Cell *127*, 1361–1373.

Brosh, R., and Rotter, V. (2009). When mutants gain new powers: news from the mutant p53 field. Nat. Rev. Cancer *9*, 701–713.

Carr, S.M., Munro, S., Zalmas, L.P., Fedorov, O., Johansson, C., Krojer, T., Sagum, C.A., Bedford, M.T., Oppermann, U., and La Thangue, N.B. (2014). Lysine methylation-dependent binding of 53BP1 to the pRb tumor suppressor. Proc. Natl. Acad. Sci. USA *111*, 11341–11346.

Case, D.A., Cheatham, T.E., 3rd, Darden, T., Gohlke, H., Luo, R., Merz, K.M., Jr., Onufriev, A., Simmerling, C., Wang, B., and Woods, R.J. (2005). The Amber biomolecular simulation programs. J. Comput. Chem. *26*, 1668–1688.

Charier, G., Couprie, J., Alpha-Bazin, B., Meyer, V., Quemeneur, E., Guerois, R., Callebaut, I., Gilquin, B., and Zinn-Justin, S. (2004). The Tudor tandem of 53BP1: a new structural motif involved in DNA and RG-rich peptide binding. Structure *12*, 1551–1562.

Cheok, C.F., Verma, C.S., Baselga, J., and Lane, D.P. (2011). Translating p53 into the clinic. Nat. Rev. Clin. Oncol. *8*, 25–37.

Chuikov, S., Kurash, J.K., Wilson, J.R., Xiao, B., Justin, N., Ivanov, G.S., McKinney, K., Tempst, P., Prives, C., Gamblin, S.J., et al. (2004). Regulation of p53 activity through lysine methylation. Nature *432*, 353–360.

Cornilescu, G., Delaglio, F., and Bax, A. (1999). Protein backbone angle restraints from searching a database for chemical shift and sequence homology. J. Biomol. NMR *13*, 289–302.

Cui, G., Botuyan, M.V., and Mer, G. (2009). Preparation of recombinant peptides with site- and degree-specific lysine (13)C-methylation. Biochemistry *48*, 3798–3800.

Cui, G., Park, S., Badeaux, A.I., Kim, D., Lee, J., Thompson, J.R., Yan, F., Kaneko, S., Yuan, Z., Botuyan, M.V., et al. (2012). PHF20 is an effector protein of p53 double lysine methylation that stabilizes and activates p53. Nat. Struct. Mol. Biol. *19*, 916–924.

Dai, C., and Gu, W. (2010). p53 post-translational modification: deregulated in tumorigenesis. Trends Mol. Med. *16*, 528–536.

DeHart, C.J., Chahal, J.S., Flint, S.J., and Perlman, D.H. (2014). Extensive post-translational modification of active and inactivated forms of endogenous p53. Mol. Cell Proteomics *13*, 1–17.

Delaglio, F., Grzesiek, S., Vuister, G.W., Zhu, G., Pfeifer, J., and Bax, A. (1995). NMRPipe: a multidimensional spectral processing system based on UNIX pipes. J. Biomol. NMR *6*, 277–293.

Duggan, B.M., Legge, G.B., Dyson, H.J., and Wright, P.E. (2001). SANE (Structure Assisted NOE Evaluation): an automated model-based approach for NOE assignment. J. Biomol. NMR *19*, 321–329.

Fernandez-Capetillo, O., Chen, H.T., Celeste, A., Ward, I., Romanienko, P.J., Morales, J.C., Naka, K., Xia, Z., Camerini-Otero, R.D., Motoyama, N., et al. (2002). DNA damage-induced G2-M checkpoint activation by histone H2AX and 53BP1. Nat. Cell Biol. *4*, 993–997.

Fnu, S., Williamson, E.A., De Haro, L.P., Brenneman, M., Wray, J., Shaheen, M., Radhakrishnan, K., Lee, S.H., Nickoloff, J.A., and Hromas, R. (2011). Methylation of histone H3 lysine 36 enhances DNA repair by nonhomologous end-joining. Proc. Natl. Acad. Sci. USA *108*, 540–545.

Fradet-Turcotte, A., Canny, M.D., Escribano-Diaz, C., Orthwein, A., Leung, C.C., Huang, H., Landry, M.C., Kitevski-LeBlanc, J., Noordermeer, S.M., Sicheri, F., and Durocher, D. (2013). 53BP1 is a reader of the DNA-damage-induced H2A Lys 15 ubiquitin mark. Nature *499*, 50–54.

Gatchalian, J., Futterer, A., Rothbart, S.B., Tong, Q., Rincon-Arano, H., Sanchez de Diego, A., Groudine, M., Strahl, B.D., Martinez, A.C., van Wely, K.H., and Kutateladze, T.G. (2013). Dido3 PHD modulates cell differentiation and division. Cell Rep. *4*, 148–158.

Güntert, P. (2004). Automated NMR structure calculation with CYANA. Methods Mol. Biol. *278*, 353–378.

Huang, J., and Berger, S.L. (2008). The emerging field of dynamic lysine methylation of non-histone proteins. Curr. Opin. Genet. Dev. *18*, 152–158.

Huang, J., Perez-Burgos, L., Placek, B.J., Sengupta, R., Richter, M., Dorsey, J.A., Kubicek, S., Opravil, S., Jenuwein, T., and Berger, S.L. (2006). Repression of p53 activity by Smyd2-mediated methylation. Nature *444*, 629–632.

Huang, J., Sengupta, R., Espejo, A.B., Lee, M.G., Dorsey, J.A., Richter, M., Opravil, S., Shiekhattar, R., Bedford, M.T., Jenuwein, T., and Berger, S.L. (2007). p53 is regulated by the lysine demethylase LSD1. Nature *449*, 105–108.

Huang, J., Dorsey, J., Chuikov, S., Zhang, X., Jenuwein, T., Reinberg, D., and Berger, S.L. (2010). G9a and Glp methylate lysine 373 in the tumor suppressor p53. J. Biol. Chem. *285*, 9636–9641.

Huyen, Y., Zgheib, O., Ditullio, R.A., Jr., Gorgoulis, V.G., Zacharatos, P., Petty, T.J., Sheston, E.A., Mellert, H.S., Stavridi, E.S., and Halazonetis, T.D. (2004). Methylated lysine 79 of histone H3 targets 53BP1 to DNA double-strand breaks. Nature *432*, 406–411.

Jha, D.K., and Strahl, B.D. (2014). An RNA polymerase II-coupled function for histone H3K36 methylation in checkpoint activation and DSB repair. Nat. Commun. *5*, 3965.

Johnson, B.A., and Blevins, R.A. (1994). NMR View: a computer program for visualization and analysis of NMR data. J. Biomol. NMR *4*, 603–614.

Kachirskaia, I., Shi, X., Yamaguchi, H., Tanoue, K., Wen, H., Wang, E.W., Appella, E., and Gozani, O. (2008). Role for 53BP1 Tudor domain recognition of p53 dimethylated at lysine 382 in DNA damage signaling. J. Biol. Chem. *283*, 34660–34666.

Kim, J., Daniel, J., Espejo, A., Lake, A., Krishna, M., Xia, L., Zhang, Y., and Bedford, M.T. (2006). Tudor, MBT and chromo domains gauge the degree of lysine methylation. EMBO Rep. *7*, 397–403.

Lee, J., Thompson, J.R., Botuyan, M.V., and Mer, G. (2008). Distinct binding modes specify the recognition of methylated histones H3K4 and H4K20 by JMJD2A-tudor. Nat. Struct. Mol. Biol. *15*, 109–111.

Levine, A.J., and Oren, M. (2009). The first 30 years of p53: growing ever more complex. Nat. Rev. Cancer *9*, 749–758.

Mer, G., Bochkarev, A., Gupta, R., Bochkareva, E., Frappier, L., Ingles, C.J., Edwards, A.M., and Chazin, W.J. (2000). Structural basis for the recognition of DNA repair proteins UNG2, XPA, and RAD52 by replication factor RPA. Cell *103*, 449–456.

Mujtaba, S., He, Y., Zeng, L., Yan, S., Plotnikova, O., Sachchidanand, Sanchez, R., Zeleznik-Le, N.J., Ronai, Z., and Zhou, M.M. (2004). Structural mechanism of the bromodomain of the coactivator CBP in p53 transcriptional activation. Mol. Cell *13*, 251–263.

Muller, P.A., and Vousden, K.H. (2013). p53 mutations in cancer. Nat. Cell Biol. *15*, 2–8.

Musselman, C.A., Mansfield, R.E., Garske, A.L., Davrazou, F., Kwan, A.H., Oliver, S.S., O'Leary, H., Denu, J.M., Mackay, J.P., and Kutateladze, T.G. (2009). Binding of the CHD4 PHD2 finger to histone H3 is modulated by covalent modifications. Biochem. J. *423*, 179–187.

Musselman, C.A., Avvakumov, N., Watanabe, R., Abraham, C.G., Lalonde, M.E., Hong, Z., Allen, C., Roy, S., Nunez, J.K., Nickoloff, J., et al. (2012a). Molecular basis for H3K36me3 recognition by the Tudor domain of PHF1. Nat. Struct. Mol. Biol. *19*, 1266–1272.

Musselman, C.A., Ramirez, J., Sims, J.K., Mansfield, R.E., Oliver, S.S., Denu, J.M., Mackay, J.P., Wade, P.A., Hagman, J., and Kutateladze, T.G. (2012b). Bivalent recognition of nucleosomes by the tandem PHD fingers of the CHD4 ATPase is required for CHD4-mediated repression. Proc. Natl. Acad. Sci. USA *109*, 787–792.

Pai, C.C., Deegan, R.S., Subramanian, L., Gal, C., Sarkar, S., Blaikley, E.J., Walker, C., Hulme, L., Bernhard, E., Codlin, S., et al. (2014). A histone H3K36 chromatin switch coordinates DNA double-strand break repair pathway choice. Nat. Commun. *5*, 4091.

Panier, S., and Boulton, S.J. (2014). Double-strand break repair: 53BP1 comes into focus. Nat. Rev. Mol. Cell Biol. *15*, 7–18.

Rappold, I., Iwabuchi, K., Date, T., and Chen, J. (2001). Tumor suppressor p53 binding protein 1 (53BP1) is involved in DNA damage-signaling pathways. J. Cell Biol. *153*, 613–620.

Roy, S., Musselman, C.A., Kachirskaia, I., Hayashi, R., Glass, K.C., Nix, J.C., Gozani, O., Appella, E., and Kutateladze, T.G. (2010). Structural insight into p53 recognition by the 53BP1 tandem Tudor domain. J. Mol. Biol. *398*, 489–496.

Shi, X., Kachirskaia, I., Yamaguchi, H., West, L.E., Wen, H., Wang, E.W., Dutta, S., Appella, E., and Gozani, O. (2007). Modulation of p53 function by SET8-mediated methylation at lysine 382. Mol. Cell *27*, 636–646.

Strahl, B.D., and Allis, C.D. (2000). The language of covalent histone modifications. Nature *403*, 41–45.

Tang, J., Cho, N.W., Cui, G., Manion, E.M., Shanbhag, N.M., Botuyan, M.V., Mer, G., and Greenberg, R.A. (2013). Acetylation limits 53BP1 association with damaged chromatin to promote homologous recombination. Nat. Struct. Mol. Biol. *20*, 317–325.

Tsui, V., and Case, D.A. (2000). Theory and applications of the generalized Born solvation model in macromolecular simulations. Biopolymers *56*, 275–291.

Vousden, K.H., and Lane, D.P. (2007). p53 in health and disease. Nat. Rev. Mol. Cell Biol. *8*, 275–283.

Ward, I., Kim, J.E., Minn, K., Chini, C.C., Mer, G., and Chen, J. (2006). The tandem BRCT domain of 53BP1 is not required for its repair function. J. Biol. Chem. *281*, 38472–38477.

West, L.E., Roy, S., Lachmi-Weiner, K., Hayashi, R., Shi, X., Appella, E., Kutateladze, T.G., and Gozani, O. (2010). The MBT repeats of L3MBTL1 link SET8-mediated p53 methylation at lysine 382 to target gene repression. J. Biol. Chem. *285*, 37725–37732.

Wishart, D.S., and Sykes, B.D. (1994). The 13C chemical-shift index: a simple method for the identification of protein secondary structure using 13C chemical-shift data. J. Biomol. NMR *4*, 171–180.

Zgheib, O., Pataky, K., Brugger, J., and Halazonetis, T.D. (2009). An oligomerized 53BP1 tudor domain suffices for recognition of DNA double-strand breaks. Mol. Cell Biol. *29*, 1050–1058.

Zhang, X., Wen, H., and Shi, X. (2012). Lysine methylation: beyond histones. Acta Biochim. Biophys. Sin. (Shanghai) *44*, 14–27.

Zwahlen, C., Legault, P., Vincent, S.J.F., Greenblat, J., Konrat, R., and Kay, L.E. (1997). Methods of measurements of intermolecular NOEs by multinuclear NMR spectroscopy: application to a bacteriophage N-peptide/box B RNA complex. J. Am. Chem. Soc. *119*, 6711–6721.